Informes Técnicos Ciemat **1089**
Septiembre, 2006

Magnetic Shear and Transport in ECRH Discharges of the TJ-II under Ohmic Induction

D. López-Bruna
F. Castejón
J. A. Romero
T. Estrada
F. Medina
M. Ochando
A. López-Fraguas
E. Ascasíbar
J. Herranz
E. Sánchez
E. de la Luna
I. Pastor

Laboratorio Nacional de Fusión por Confinamiento Magnético

1. *Introduction*

One of the difficulties in identifying transport mechanisms in stellarator plasmas is that all of them seem to contribute on a comparable footing. There is little doubt that the confining properties are related to particle orbits and collisional transport [**1**, **2**]. The breaking of vacuum magnetic flux surfaces in the presence of plasma currents is also proven to have an impact in confinement (see [**3**] and references therein). ExB turbulence is known to be present even in low β stellarator machines, although quantifying its effect on transport has turned out to be extremely difficult. A notable effort in identifying the origin and incidence on transport of drift wave turbulence was done in the early 90's by the ATF group [**4**], when experiments aimed at identifying dissipative trapped electron modes (DTEM) were performed. Support from theory [**5**] indicated that the magnetic shear, $\hat{s} = -(\rho/\iota)(d\iota/d\rho)$ being ρ a flux surface coordinate and ι the rotational transform in radians, may be important in stabilising DTEM. Later, a work by Waltz and Boozer [**6**] warned that a local, non flux surface magnitude termed *local* shear, could be the true stabilising magnitude especially in low $\hat{s}$ machines like the heliac and helias stellarators. A number of theoretical and numerical works (see, e. g. [**7**]) supported the assumed importance of local magnetic shear in stellarators, still not ruling out the possible effect of $\hat{s}$ [**8**].

The effect of $\hat{s}$ has been considered in other machines from different perspectives. In the Heliotron-E, a large shear machine, they found that changing the ratios between toroidal or vertical, and helical magnetic fields (B_t/B_h and B_v/B_h) in ECRH plasmas (also neutral-beam heated), the particle and energy confinement can be optimized [**9**]. These ratios affect the rotational transform and shear. Their calculations on particle losses agreed with the optimum magnetic axis shift (controlled via B_v/B_h), but studies related directly to the magnetic shear were only dedicated to its effect on heating [**10**]. In a shearless stellarator, the Wendelstein 7-AS, much work was done to investigate the conditions (in terms of edge rotational transform) of optimum confinement. Particularly, the technique of weak ohmic induction was used to study turbulence in such conditions [**11**]. A clear relation between confinement and rotational transform was found, but the work did not focus on the possible relationship between transport and magnetic shear.

TJ-II is a stellarator of the heliac type [**12**]. This kind of magnetic trap was conceived as a shearless, high rotational transform device with good MHD properties [**13**]. Its vacuum configurations span edge values of the rotational transform $\imath = \iota/2\pi$ in the interval 0.9 to 2.2 and the machine is commonly operated slightly above the 3/2 value. A brief overview of effects related to rational surface placement in ECRH plasmas of the TJ-II device can be found in Ref. [**14**] and references therein. Several experiments in TJ-II were dedicated to examine the effect of ohmically inducing plasma currents [**15**, **16**], which showed a link between plasma current and transport. It was argued that the simple presence of low order rational values of the rotational transform was not likely to explain such link. Further analysis is now devoted to perform local analysis on the evolution of transport and rotational transform profiles. Particularly, since the effect of global shear in stellarators remains to be clarified, it is the purpose of this work to inform on the relationship between $\hat{s}$ and transport in our experimental conditions. For instance, if $\hat{s}$ is a relevant quantity for transport, it would be of definite interest to perform new calculations on drift wave turbulence where configurations with varying $\hat{s}$ are explored to verify wether or not the magnetic shear, aside from the local shear, can have an impact on turbulent transport in stellarator machines. It is also worth noting that moderate values of $\hat{s}$ can be externally controlled.

It is important to realize that there are two different aspects of the plasma response to an evolving rotational transform that we intend to separate: first, there are fast changes (compatible with MHD timescales) in the plasma response that have been studied and considered in relation with low order rational values of $\imath$. Second, there is the link just mentioned between plasma transport and plasma current. Since these two aspects must be distinguished, we remind briefly the first one with two examples in the next paragraph and focus on the second thereafter.

There is a rather well characterised effect of the magnetic configuration on the appeareance/disappeareance of a hot core in TJ-II plasmas heated by electron-cyclotron-resonant waves (see Refs. [**17**, **18**, **19**]). In brief, the experiments show that a low order rational value of the rotational transform in the region of ECR power deposition sets conditions for heat accumulation. The phenomenon is very fast –in kinetic, rather than transport, timescales– and thus can be found transiently or even in the manner of an oscilatory process if the conditions are marginal, as seen when the discharge evolves in the background of a vacuum ι-profile that grazes a low order rational value in the core region. The explanation, albeit still awaiting quantitative support from detailed modelling, is consistent with the notion of radial electric field enhancement due to the large unbalance between electron and ion fluxes when a region with broken magnetic symmetry overlaps the power deposition zone (where electron pump out mechanisms are active [**19**]). This phenomenon must be distinguished from the so called N-ITB [**20**], where a bifurcation to better heat confinement happens due to a change in neoclassical root of the radial electric field. A second example of phenomenon very likely due to MHD processes is the ELM-like activity identified in TJ-II plasmas similar to those pertaining to the present work. The necessary ingredient for such events to occur is that a low order rational of ι is present in the region of steepest pressure gradients [**21**]. However, this condition is not sufficient as experiments with ohmic induction have proven: in agreement with results from other devices (e. g. [**22**, **23**]), lowest order rationals can be present in stable discharges as long as there is enough magnetic shear. This also agrees with early calculations for the TJ-II [**24**]. Thus, the natural $\iota = \mathsf{n}/\mathsf{m} = 4/2$ makes barely possible sustaining an ECRH plasma in TJ-II, while if this same rational is moved into the plasma with transformer-induced currents the discharge is easily maintained. This is a well-explored effect of stabilization of MHD modes via magnetic shear (see, e.g. [**3**]). From experiments of this kind in the TJ-II it is known that a small net ohmic plasma current ≈ -2 kA or, in terms of magnetic shear, small values $\hat{s} \sim 0.1$, are enough to make the deletereous effects of lowest order rationals essentialy disappear.

As mentioned above, there is a second aspect of plasma response to moderate ohmic currents: all the studied ECRH plasmas in the TJ-II evolving under ohmic induction show a link between net plasma current and confinement [**15**, **16**]. The limitations imposed by the ECRH cut-off density in the TJ-II impede a study of maximum performance given the available ECRH power and transformer flux change, but within such limits it is clear that the pressure profiles narrow smoothly as the ohmic current increases from zero; and conversely: the pressure broadens following roughly the magnitude of negative currents. For high enough (~ 7 kA) net currents of either sign the plasma improves confinement. Any ideas aimed at explaining these findings must be congruent with the following facts:

(1) Vacuum ι profiles are almost shearless. In the presence of plasma -but without any induction or other means of toroidal current drive- there is a net $I_p \lesssim 1$ kA, attributed to diamagnetic and kinetic effects, that seems to alter the vacuum ι only weakly [**17**, **25**]. Therefore, positive/negative ohmic currents increase/decrease the magnetic shear from nearly zero.
(2) The induced plasma currents are high enough that, during the induction process, lowest order rational values of ι are moved throughout most of the plasma for *both* positively and negatively induced loop voltages.
(3) The plasmas studied are characterised for having a core ($\rho \lesssim 0.5$ where, roughly, 50% of the thermal energy is stored) in the long-mean-free-path regime of collisionalities. We are considering such regime for $\nu^* = (\nu R_0)/(v\iota) \lesssim 10^{-2}$, where R_0 is the major radius, ν is the collision frequency and v is the thermal speed (see calculations of neoclassical transport regimes in Ref. [**26**]). Transport in this region is affected by particle orbit properties.

In addition, the plasma β ($< 0.3\%$) and magnetic well (the specific volume falls approximately 2% from core to edge) do not change during the evolution of these ECRH discharges. This is a valid approximation if we assume that the flux surface geometry is only slightly modified by the induced plasma currents.

This paper informs on the relationship between transport in TJ-II ECRH plasmas with boronised wall and the magnetic shear $\hat{s}$ imposed by ohmically inducing plasma currents. Both concepts, transport and magnetic shear, involve some kind of modelling. The magnetic shear depends, indeed, on the actual current density

profile. In Sec. 2 we make use of detailed calculations based on the geometry of the TJ-II to show that Spitzer formula corrected by the fraction of passing particles offers appropriate values for the plasma conductivity in the TJ-II. In Sec. 3 we comment a set of three discharges to illustrate the effects of ohmic induction in our plasmas. Based on the results of Sec. 2 we can face the calculation of the evolution of the rotational transform and its derivative $\hat{s}$ in Sec. 4, which allows us to gain confidence on our representation of the resistivity by comparison with experimental time traces. We discuss heat and particle transport in terms of ι and $\hat{s}$ in Sec. 5. A brief final comments and the summary are left for Sec. 6.

2. *Loop voltage and conductivity*

One of the main benefits of working with plasmas under moderate induction is that the uncertainties of the ι profile are considerably alleviated, especially when part of the interest of our work relies on its radial derivative ($\hat{s}$). The reason is as follows: the vacuum ι is basically flat, which makes ι rather sensitive to the bootstrap current density when the plasma is present. Our knowledge of the bootstrap current density profile is that it increases ι near the core while having a small but opposite effect in more or less the outer half of the plasma [**27**, **28**, **29**]. However, the contribution to the net plasma current from this outer region, which may be attributed to the "helical" part of the bootstrap current [**30**], can be comparable to that from the inner region because it occupies a larger volume. Thus, net plasma currents of ECRH plasmas in TJ-II can be either positive or negative. Their magnitude depends, among other factors, on wall conditioning [**31**], a reason why it makes sense giving an indication of its importance in the present case. Fig. 1 shows net plasma currents found in reference discharges (no induction nor ECRH current drive) versus the line density of the discharge during the experimental campaigns when OH experiments were performed. The data have been averaged during the plateau of each discharge and the error bars indicate standard deviation. Apparently, larger densities enhace the negative values of plasma current density. As seen, net plasma currents in reference discharges pertaining this work range from ≈ 0.1 kA at $\bar{n}_e \approx 0.4 \cdot 10^{19}$ m^{-3} to ≈ -0.3 kA at $\bar{n}_e \approx 0.7 \cdot 10^{19}$ m^{-3}. These values are to be compared with the ohmically induced values up to 10 kA and concentrated in the inner half of the plasma, where T_e is largest. In summary, although we acknowledge that the bootstrap current density profile is unknown, we shall consider that its influence is of second importance in the results that follow. All calculations of the evolution of ι in this work consider the ohmic induction alone.

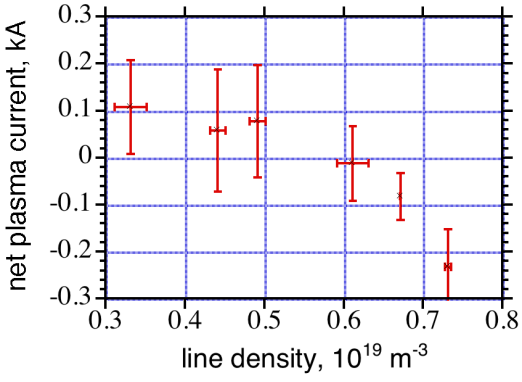

FIGURE 1. *Net experimental plasma current in reference discharges (no induction or current drive) versus line average density. The data are averages over* ~ 150 *ms in the plateau of the discharges. Error bars indicate standard deviation of the raw data.*

We have used several means to calculate the evolution of ι in the TJ-II discharges with induced currents. In

a first work [**15**], the evolution of the poloidal magnetic field was obtained in cylindrical geometry imposing the experimental values of the ramps in the inductor coils, dI_{OH}/dt, and using a mutual induction coefficient based on the design parameters of TJ-II. Now we have included the flux-surface averaged metrics of the TJ-II for the magnetic configuration of our experiments in these calculations. Particularly, a proper evaluation of radial derivatives is necessary because we are interested in magnitudes that envolve such derivatives (like interpretative transport coefficients and magnetic shear). Since the TJ-II has a rather large (> 7) aspect ratio, we assume that the evolution of ι can be, to a good approximation, calculated with the ASTRA package [**32**], where the description of the geometry is forcedly axisymmetric. We have calculated the flux surface averages of several metric magnitudes (specific volume, squared gradient of the flux surface label, diagonal metric elements) and used them as input data in ASTRA. The vacuum geometry is used throughout all calculations.

The loop voltage diagnostic is taken in a circuit approximately coincident with the central conductor in the TJ-II. It consists of the voltage drop, V_l, along the metal casing that protects this coil and the helical conductor that winds around it. Numerical calculations allow us considering the loop voltage diagnostic as a measurement of V_p, the plasma loop voltage [**33**], under conditions of variable I_{OH} and steady-state plasma current. Here we understand the plasma loop voltage, relevant to the estimate of parallel electric fields $E_\parallel$, to be the circulation of $E_\parallel$ along a sufficiently large number of turns following a magnetic field line with irrational winding number and divided by the number of turns. Thus, $E_\parallel$ is a flux surface function and the parallel plasma current density is $J_\parallel = \sigma_\parallel E_\parallel = \sigma_\parallel V_p/L$, where L is taken to be the length of one toroidal turn of a magnetic field line given a magnetic surface. This length is practically the same for every magnetic flux surface in the TJ-II, $L \approx 11$ m.

The calculations of the evolution of ι have been performed with ASTRA: we impose the vacuum ι taken from TJ-II configuration data and calculate the modification using the measured I_p as boundary condition for the transport equation that evolves the magnetic poloidal flux,

$$\frac{\partial \Psi}{\partial t} = L E_\parallel = \frac{L}{\sigma_\parallel B_0} \langle \mathbf{J} \cdot \mathbf{B} \rangle .$$

Observe that in this expression we have not taken into account plasma currents other than transformer induced. Under this assumption, the calculated loop voltage ($V_p = LE_\parallel$) must be coincident with the measured loop voltage V_l in steady state. Therefore, using the experimental I_p and V_l we can make an estimation of the parallel conductivity $\sigma_\parallel$. Since our experimental data are integral values, we must assume a model for the radial dependence. Differences between Spitzer conductivity, σ^{SP}, and modified values after considering the trapped particle population are long known and show that the modifications can be very important in the plasma edge, where the trapped fraction f_t is large [**34**]. In our case most of the current flows in regions inside $\rho \approx 0.4$, but we shall still consider this modification. Therefore we adopt, as in previous works on the TJ-II, a plasma condutivity that obbeys Spitzer's formula multiplied by the fraction of passing particles, $\sigma = \sigma^{SP}(1 - f_t)$, where $f_t \propto \sqrt{\rho}$. In addition, we set a free constant C so that

$$\sigma_\parallel = C\sigma^{SP}(1 - f_t).$$

In Fig. 2 we show the experimental value V_l for TJ-II discharge #8714 and the calculated values of the rotational transform in the magnetic axis, $\iota(0)$, and V_p. A linear ramp $dI_{OH}/dt = -32.4$ kA/s starts at $t = 1160$ ms. A fair coincidence between V_l and V_p is obtained with $C = 0.8$ in our expresion above for $\sigma_\parallel$, which means that the Spitzer formula is addequate for the conductivity of ECRH plasmas in the TJ-II, at least in terms of integral values (given the uncertainties in these calculations and measurements, we consider this value to be compatible with $C = 1$). $\sigma_\parallel$ may behave differently to Spitzer's formula near the magnetic axis, where the ECRH power density is highest. Being this a small region that, moreover, we exclude from our

analysis, we keep the density and temperature dependences from σ^{SP} for the whole plasma. Note also that, even though our justification for imposing $V_p = V_l$ is only valid in steady state, the evolution of V_p matches quite well the measured evolution V_l. Let us finish this section recalling the main points: our estimate of the plasma conductivity is based on (i) the assumption that TJ-II ECRH plasmas obbey the main dependences of Spitzer resistivity corrected by the fraction of passing particles and (ii) the knowledge of I_p and $V_p = V_l$ in steady state.

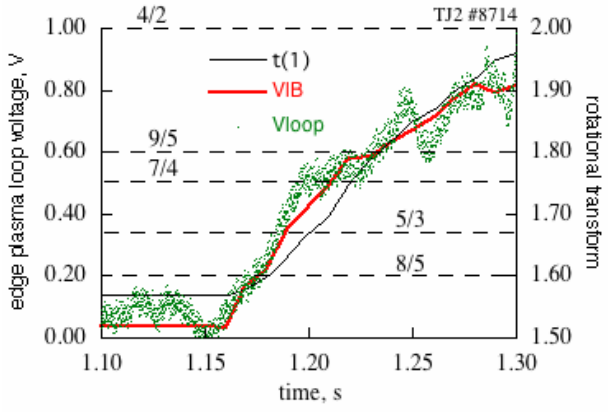

FIGURE 2. *Evolution of the calculated boundary value of induced voltage (thick red line) and the measured plasma loop voltage (dots) for TJ-II discharge #8714 with positive induction. Also shown is the calculated core rotational transform (thin black line) using as boundary condition the experimental net plasma current. Low order rational values of ι are indicated above the corresponding horizontal dashed lines.*

3. *Experiments with ohmic induction*

Here we show a selection of our experiments with ohmic induction and ECRH (200 kW of injected power at 53.2 GHz, 2nd harmonic, X-mode of polarisation) in the TJ-II device. As noted in previous works [**15**, **16**], the response of these plasmas to the process of weak ohmic induction is systematic. Our present choice of discharges responds to the fact that they share a same current ramp in the OH coils (therefore inducing a same loop voltage in the absence of plasma) in conditions of similar line densities, but the ramps have opposite sign. In addition, there is another reference discharge without OH currents. The three discharges belong to the same operation day: they were performed in a time span of about 2 h and are supposed to operate under equivalent wall conditions.

Fig. 3 shows raw data from several diagnostics for the three discharges selected: discharge #7036, with negative ramp in the OH coils and thus positive induced loop voltage (line with squares); #7034 without OH induction (crosses); and #7046, with negative induction (circles). Shown are, from top to bottom, the net plasma current as detected with the Rogowskii loops, the line average density, the intensity of H_α emission coming from the position where the working gas (H) is puffed (converted to net electron source units after calibration), and the H_α emission coming from the plasma edge at a position far from the gas puffing valve (a measurement related to recycling from the wall).

Unfortunately, the line density for discharge #7046 is smaller at the beginning of the ramp. In the TJ-II, the difficulty in starting negative induction in ECRH discharges with densities $\gtrsim 0.5 \cdot 10^{19}$ m^{-3} is that the plasma is pushed towards ECRH cut-off density ($\approx 1.7 \cdot 10^{19}$ m^{-3}, normally corresponding to line density $\approx 1.2 \cdot 10^{19}$ m^{-3} in these plasmas) as the plasma current intensity grows. Actually, it can be appreciated

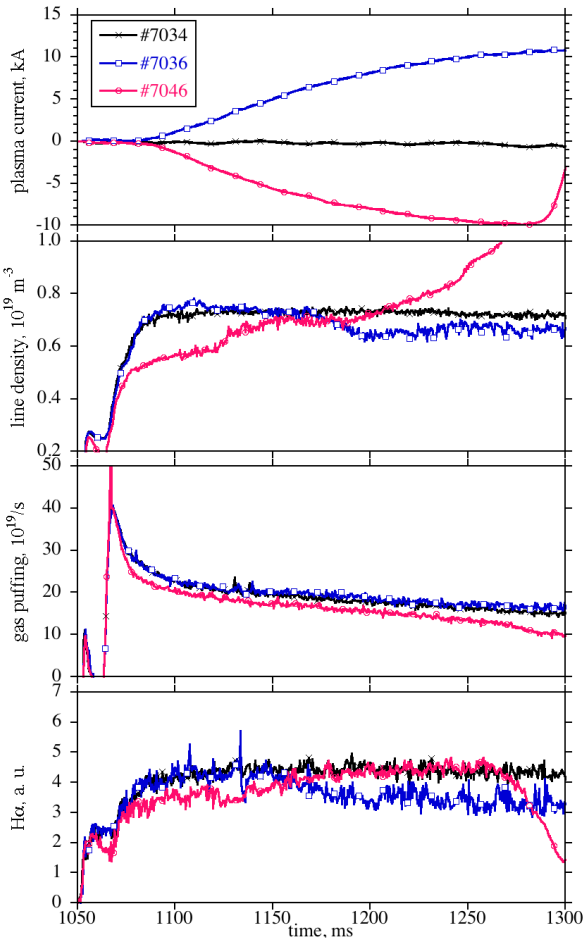

FIGURE 3. *Time traces of several diagnostics for TJ-II ECRH discharges #7036 ($dI_{OH}/dt = -28$ kA/s; squares), #7046 ($dI_{OH}/dt = +28$ kA/s; circles) and #7034 (reference, $I_{OH} = 0$; crosses). Shown are, from top to bottom: net plasma current, line average density, and H_α light intensity from the gas puffing position (converted to electrons per second) and from a toroidal position far from the gas puffing sector.*

in Fig. 3 that the plasma is headed to cut-off as of $t \approx 1250$ ms. Despite this, the general trends in the behaviour of the plasma can be easily observed: in comparison with the reference case, the plasma becomes more dense with negative induction and conversely.

The calculated evolution of the plasma energy content and the energy confinement time is based on experimental values of the electron temperature and density profiles assuming almos flat ion temperature profiles [**35**] with maximum T_i between 0.09 and 0.10 keV. The reconstruction of the profiles is done, briefly, as follows: a multichannel Electron Cyclotron Emission (ECE) diagnostic absolutely calibrated [**36**] (and systematically compared with Thomson Scattering [**37**] measurements when available) is used to obtain the evolution of $T_e(\rho)$. Time dependent density profiles were estimated using local soft X ray (SXR) emissivities, T_e profiles as obtained from ECE, and Thomson scattering profiles to take into account the impurity profile. At the plasma edge, where SXR signals are not available, profiles obtained by reflectometry were used. We have checked that the time evolution of the total radiation and the line density are coincident, which supports the hypothesis of constant effective charge for the reconstruction of n_e profiles from SXR. These profiles are normalized to give the experimental line integral. To estimate energy, τ_E, and particle, τ_p, confinement times the knowledge of the sources is mandatory. In the case of τ_E, we assume a gaussian shaped ECRH power

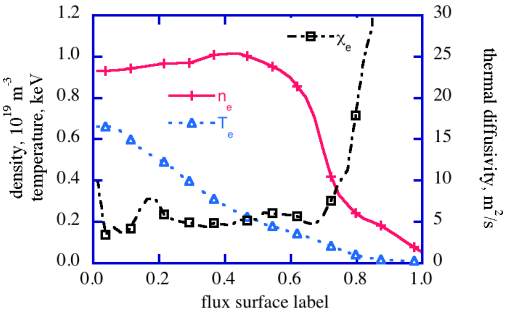

FIGURE 4. *Experimental steady state profiles of density (crosses) and electron temperature (triangles) for reference discharge #7034; and calculated thermal diffusivity (squares).*

deposition profile considering its integral to be compatible with the calorimetric measurements of injected power. This value is then corrected assuming 15% port-through losses. Since our conclusions rely on having constant deposition, we do not include an estimate of absorption efficiency, but from bolometric signals we infer that the absorption in these discharges is constant. Therefore, we give sense to the relative variation of τ_E, within and amongst discharges, in the knowledge that our τ_E is underestimated. Also, our estimate of thermal transport coefficients assumes that most of the power is deposited inside $\rho \approx 0.3$. In the case of τ_p we face the difficulty associated with the neutral fluxes coming from recycling processes in the chamber wall. It has been shown in Fig. 3 that H_α light intensity coming from the gas puffing zone behaves in a smooth way. The corresponding H_α monitors are calibrated to give an estimation of Hydrogen atoms entering the plasma via gas puffing (note that discharge #7046 has a slightly reduced puffing precisely to avoid a rapid rise to cut-off density). However, recycling processes should be incorporated in transport calculations considering the relationship between outward particle flows, recycling factor at the wall and efficiency of the recycling, something out of our present possibilities. Our choice has been to consider the output of the ASTRA package for wall neutrals as guidance to the neutral distribution inside the plasma. The values of energy of warm and cold wall neutrals and corresponding edge densities are chosen to give, for the reference discharge #7034, a net source of the order of the gas puffing value of Fig. 3, which only considers the externally controlled gas source. This is a compromise between a physical model and a completely arbitrary particle source. In some cases, which will be indicated when needed (Sec. 5), we take the particle source profile found in discharge #7034 as a fixed profile for different discharges and times. In those cases, the particle diffusivities can be considerred as a different way to look at density gradients.

4. *Evolution of the rotational transform*

The large bumpiness of the magnetic field in TJ-II configurations suggests that plasma current densities associated to anomalous parallel resistivity are small [**38**] in comparison with Spitzer ($\sigma E_\parallel$) currents in OH experiments. Therefore, we only expect considerable modifications of the rotational transform profile near the core, where the pressure gradient, mean free path and toroidal symmetry are largest probably giving, in agreement with present calculations for the TJ-II [**29**], a positive bootstrap current density roughly proportional to $\nabla(nT_e)$. The electron density obtained from the Thomson diagnostic (crosses) and the temperature obtained from ECE and Thomson diagnostics (triangles) corresponding to the reference discharge #7034 (see Fig. 3) are plotted in Fig. 4 together with the calculated steady state thermal difussivity. These profiles are representative of the plasmas we are considering in OH experiments and of those considered in the referenced estimates of bootstrap current densities. We now calculate (Fig. 5) the ι profile in the presence of a model bootstrap current density profile. Its toroidal flux gives a net value of -0.5 kA. This model profile was used to investigate MHD stability in the TJ-II [**39**] and is qualitatively equivalent to the profiles found

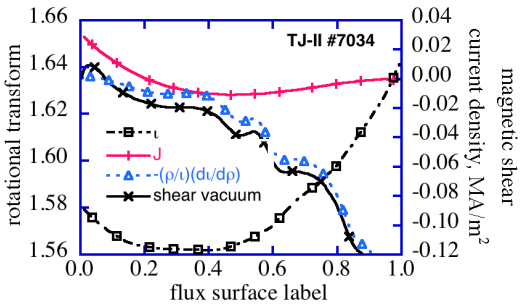

FIGURE 5. *Calculated steady state rotational transform (squares) and magnetic shear (triangles) that correspond to a model bootstrap plasma current density profile (pluses). The vacuum shear is also shown (crosses). The net plasma current in this calculation is -0.5 kA.*

in Ref. [**29**]. As we soon shall see, modifications to the ι-profile and, very especially, the magnetic shear, due to OH induction are considerably larger. Therefore, despite being uncertain, bootstrap current profiles are unimportant in our OH experiments as far as we can reasonably state. Note also that there is some net vacuum magnetic shear in most of the minor radius, which accounts for the asymmetry of the values of $|\hat{s}|$ reached in cases of symmetric positive and negative net plasma currents.

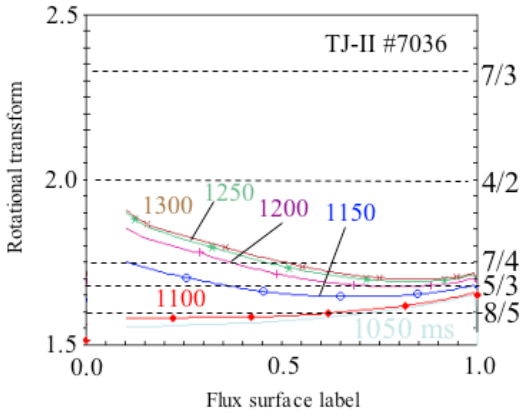

FIGURE 6. *Evolution of the rotational transform under a constant ramp of -28 kA/s in TJ-II discharge #7036.*

The calculated evolution of the rotational transform for TJ-II discharges #7036 and #7046 is presented respectively in Figs. 6 and 7. A few horizontal dashed lines show lowest order ($\mathsf{m} \leq 5$) rational values of ι. In both cases low order rationals scan large regions through the plasma radius. It is important to realize that they are, however, reached with finite magnetic shear with two exceptions to be kept in mind: (i) the $\iota = 3/2$ rational with negative currents (Fig. 7); and (ii) all rationals abandoning the plasma near the edge for positive currents (Fig. 6). Figures 8 and 9 show the corresponding time traces of several diagnostics: in the top panel, the calculated values of ι at $\rho = 0.1$ (solid line) and $\rho = 1.0$ (dashed line) are displayed along with vertical bars drawn to mark the times at which the core ι reaches the labeled rationals. Next we plot an H_α signal, a central chord of soft X-rays, the central electron temperature and, at the bottom panel, a Mirnov coil signal. Here we represent with horizontal arrows the time during which the main edge rational (5/3) stays in the interval $0.8 \lesssim \rho \lesssim 1.0$ until disappearing, always according to the calculations.

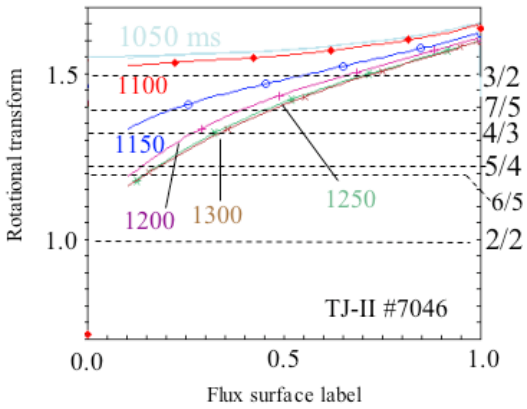

FIGURE 7. *Evolution of the rotational transform under a constant ramp of 28 kA/s in TJ-II discharge #7046.*

In general, Mirnov coil data (especially sensitive to edge phenomena) can be fairly interpreted in view of these horizontal arrows. In Fig. 6, the 5/3 rational shows up at the edge at $t \approx 1130$ ms, which may explain the bursts in the magnetic diagnostic and in the H_α, and penetrates in the plasma until $t \approx 1195$ ms, when it disappears from the finite region it occupies. The 8/5 rational disappears from the plasma at $\rho \approx 0.5; t = 1120$ ms, very soon after appearing in the core. We indicate this time with a vertical arrow in the SXR data. In Fig. 9 the magnetic signal increases amplitude quite steadily from 0.4 ($t \approx 1050$ ms) to 1.2 ($t \approx 1200$ ms) during the discharge, possibly due to the $\iota = 3/2$ approaching the edge (see also Fig. 7).

In the core region and for positive induction (Fig. 6), most of the bursty activity in H_α, $T_e(0)$ and SXR signals (Fig. 8) can be related to the presence of the 8/5, 5/3 and 7/4 rationals in the core region. The spikes as of $t \approx 1210$ ms in $T_e(0)$ are very likely the signature of the $\iota = 4/2$. To interpret the time signals in Fig. 9 (negative induction), our experience is that low order rationals start to make themselves noticeable when reaching the temperature gradient region. In particular, according to recent interpretations (see Ref. [**19**] and Sec. 1 in this article), the first jump in $T_e(0)$ in Fig. 9 is due to the $\iota = 3/2$ in the T_e gradient zone but still overlapping the ECRH power deposition, which happens soon after $t \approx 1115$ ms. The second jump in T_e may have to do with the 4/3 rational. Check Ref. [**18**] for more on these phenomena in the TJ-II. Even if the calculations lack accuracy, let us recall that we are after identifying a reason for a continuous degradation of confinement with positive induction and conversely. In Figs. 3 and 8, the descent of the SXR and line density happens around $1150 \lesssim t \lesssim 1200$ ms, precisely when the calculations of ι (Fig. 6) and the Mirnov signals do not indicate that the MHD activity should be responsible. Moreover, Figs. 3, 7 and 9 state that the plasma performance in these ECRH conditions can improve even with a scan of the $\iota = 3/2$ throughout practically the entire plasma, albeit with finite magnetic shear. Note, for example, that at $t = 1200$ ms, when the confinement starts to improve markedly, all the low order rationals labeled in Fig. 7 except the 2/2 are supposed to stay between $\rho = 0.1$ and $\rho = 0.8$.

The presence of different low order rationals is acknowledged but there is no apparent relationship between them and performance. It has been observed (e. g. [**3**]) that when a high sheared magnetic field is present, the possible negative influence of low order rationals on confinement is neutralized. Our experiments support this notion and establish values of $\hat{s} \sim 0.1$ as "high enough". We therefore turn to analyze the problem from the viewpoint of $\hat{s}$ instead of ι itself.

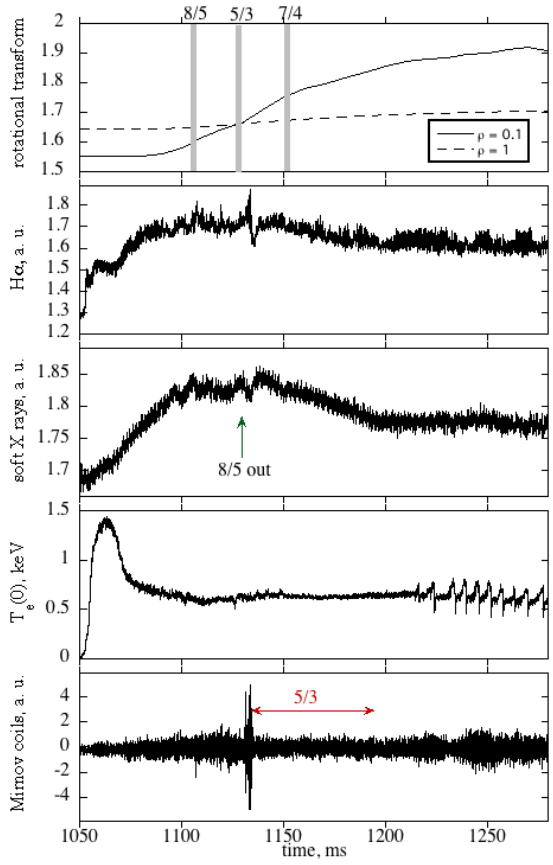

FIGURE 8. *From top to bottom, time traces of calculated core ($\rho = 0.1$) and edge rotational transform, Hα, a central chord of soft X-rays, central electron temperature and Mirnov coil signals for TJ-II discharge #7036. Vertical bars indicate the times at which ι at the core reaches low order rationals. Horizontal arrows indicate time spans at which the edge ι features low order rationals, also indicated, in the region* $0.8 \leq \rho \leq 1.0$. *See Fig. 6.*

5. *Transport analysis*

5.1. *Thermal energy*

Figs. 10 and 11 show the evolution of the magnetic shear and thermal diffusivity profiles at several times during the evolution of discharges #7036 and #7046 (see Figs. 3, 6 and 7). The plasma core and edge regions are excluded because the profile uncertainties in those extreme regions are large, especially in evaluating gradients. In the bulk plasma region ($0.2 < \rho < 0.8$) we have the uncertainties related to the difference between vacuum and true magnetic configuration, which may make the evaluation of gradients slightly different, and of course the uncertainties in the source/sink profiles. However, the detailed shape of the centered ECRH should not have importance in the region shown in Figs. 10 and 11 in relation with the estimate of thermal diffusivities χ_e. Our main assumptions here are: (i) the heat source is constant; and

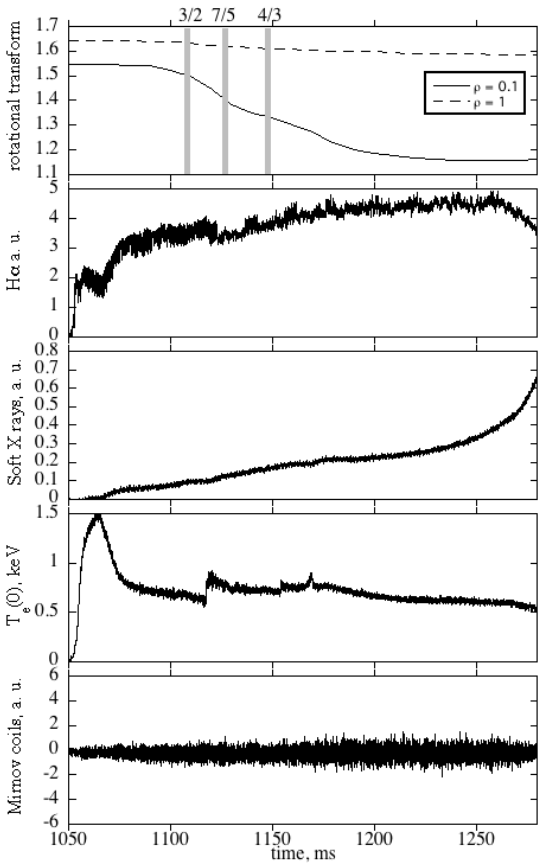

FIGURE 9. *Same as Fig. 8 for TJ-II discharge #7046. See the corresponding evolution of ι in Fig. 7.*

(ii) the geometry, even if it is not described accurately enough, accounts for a systematic error that should likewise affect all of our calculations of χ_e making the comparisons meaningful within and amongst discharges.

It is clear in Figs. 10 and 11 that $\hat{s}$ is rather uniform in the region $0.3 \leq \rho \leq 0.8$ and that the thermal diffusivity χ_e obtained from the experimental profiles evolves smoothly as $\hat{s}$ does. We note that χ_e remains more or less constant and uniform in this region for positive shear while it decreases with negative shear. The reference case, discharge #7034, has almost constant $\chi_e \approx 5$ m^2/s in most of this same region $0.3 \leq \rho \leq 0.8$ (Fig. 4) during the plateau of the discharge.

The case of positive shear (discharge #7036) develops a small region of reduced gradient in T_e near the core, which, under the assumption of constant ECRH profile, forces a peak in χ_e (Fig. 10). This kind of peak is often found in TJ-II ECRH plasmas and, in OH discharges, we have seen it developping mostly in positive induction (and shear) cases. If it corresponds to an actual local enhancement of transport, the interest is that it stays where it is born, contrary to what one would expect if it corresponds to a moving magnetic island. According to Fig. 8, the 4/2 rational shows up at $t \approx 1200$ ms. This is approximately coincident with the development of the peak in χ_e (see line with filled circles in Fig. 10). Despite this peak in χ_e, the effect on heat confinement is weak (see later).

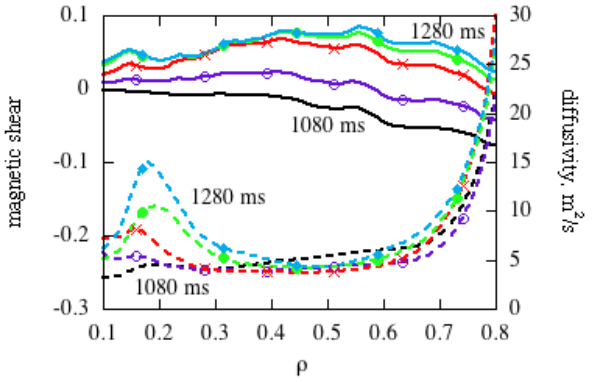

FIGURE 10. *Time evolution of the magnetic shear (solid lines) and thermal diffusivity (dashed lines) profiles in the bulk plasma of TJ-II discharge #7036 (see Fig. 6): 1080 ms, 1130 ms (open circles), 1180 ms (crosses), 1230 ms (dots), 1280 ms (diamonds) and 1280 ms (triangles).*

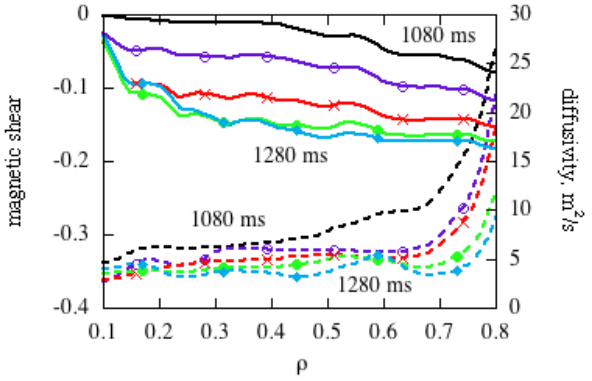

FIGURE 11. *Same as Fig. 10 for TJ-II discharge #7046.*

In the case with negative shear, Figs. 7 and 11, we see that the rational surfaces $\iota = 3/2$ and $4/3$ cross most of the confining flux surfaces. We may consider the rationals with poloidal number $\mathsf{m} = 2$ as the lowest order ones in these experiments. In consequence, low order rationals, at least in an environment of moderate global shear $\hat{s}$, do not alter heat transport in an essential way. Even if we consider that the χ_e peaking in Fig. 10 responds to the presence of the $\iota = 4/2$, we should ask why the $\iota = 3/2$ does not show up similarly in Fig. 11: either the sign of $\hat{s}$ has a drastic effect on the width of magnetic islands ascribed to low order rational values of ι, or the changes in confinement should be related to non purely MHD physics.

Turning to global transport, we estimate the evolution of the thermal energy confinement time, τ_E, and the stored plasma energy, W_{pl} (see Fig. 12). These values for the reference discharge #7034 remain practically constant at, respectively, $\tau_E = 1.8$ ms and $W_{pl} = 450$ J. As expected from Fig. 10, W_{pl} and τ_E suffer little evolution for positive induction, or shear, although the tendency is to degrade confinement. On the contrary, the energy confinement improves with negative magnetic shear within the limits of our experiments.

5.2. *Particles*

Quantitative values on particle confinement are less certain because of the lack of source terms knowledge. Nevertheless, we can make an estimate of trends in particle confinement recalling the assumption made on constant boundary conditions in the three discharges for the calculations of particle source profiles. Fig. 13 presents, with open symbols, the values of τ_p obtained with the evolving total number of electrons, $\int n_e dV$

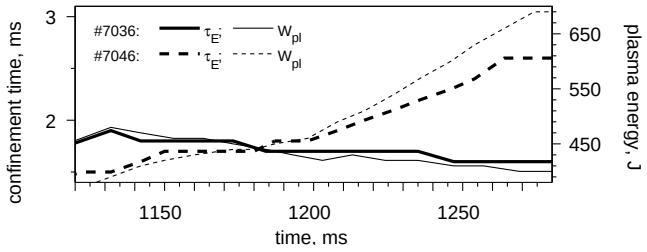

FIGURE 12. *Energy confinement time (thick lines) and plasma stored energy (thin lines) for TJ-II discharges #7036 (solid) and #7046 (dashed).*

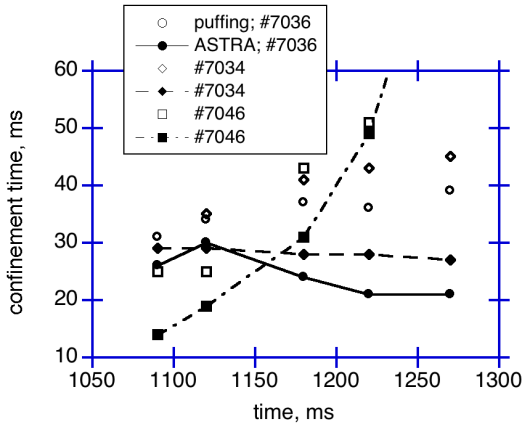

FIGURE 13. *Evolution of the electron confinement time τ_p for TJ-II discharges #7036 (circles), #7034 (diamonds) and #7046 (squares). The values of τ_p are obtained using the gas puffing alone (open symbols) and the ASTRA package for the electon source under fixed boundary conitions (filled symbols with lines).*

being V the plasma volume, and the electron source from the gas puffing rates of Fig. 3 for discharges #7036 (circles), #7034 (diamonds) and #7046 (squares). In addition, we plot (with corresponding filled symbols and lines) the values of τ_p estimated with ASTRA. The trends observed in the line density are mimmicked by the particle confinement time: positive currents degrade particle confinement and negative currents improve it. As explained in Sec. 3, the values of τ_p are not as important as their relative variation. τ_p values around 10 ms can be found in ECRH TJ-II discharges in this magnetic configuration for low injected power per particle [**40**] and therefore our numerical values may be overestimated by around a factor two. If the effective puffing efficiency remains constant, however, the data in Fig. 13 simply illustrate the results of previous works [**15**, **16**]: there is a relationship between net plasma current and particle confinement time.

One of the systematic features of our ECRH discharges with induced currents is the smooth change in density gradients [**16**]. Assuming a fixed distibution of the electron source from gas puffing, such changes can be translated into an evolving particle diffusivity D_e. Fig. 14 shows D_e in the density gradient region during the evolution of the magnetic shear, which we plot in the same figure for reference. The figure corresponds to the discharge #7046 with negative induction. The particle diffusivity decreases as $\hat{s}$ becomes more negative. When the same information is plotted for positive shear, the trends are inverted (not shown). This analysis does not consider any direct losses or convection but only diffusive transport.

It has been specified that our choice of three discharges was done for the benefit of the comparison. Let us finish this section by showing a synoptic view of confinement trends after performing the same analysis for a larger set of discharges with ohmic induction. In Figs. 15 and 16 we plot the calculated electron diffusivity D_e and heat diffusion χ_e versus $\hat{s}$ for a group of OH discharges (which includes comparable discharges #7036

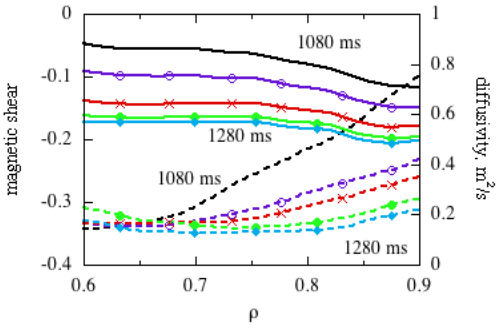

FIGURE 14. *Estimated evolution of the magnetic shear (solid lines) and the electron diffusivity (dashed lines) for discharge #7046 (see Figs. 7 and 11).*

and #7046, highlighted with larger symbols). All of them share the same heating and general conditions, although gas puffing and densities are generally different. Each symbol represents data for one discharge. The choice of $\rho = 0.75$ responds to the need of staying in a region where density transport is plausibly diffusive, which excludes the flat (or even hollow) core region, where ECRH pump out is at work), and the edge. Moreover, in Ref. [**16**] we found the region $0.6 \lesssim \rho \lesssim 0.8$, roughly the density gradient region, as a possible location for unstable drift modes related with trapped particles in the TJ-II. In our analysis this is the range in minor radius where the changes in transport are more significant and it is thus appropriate looking for a relationship between transport and shear in this zone. To draw Fig. 15 we have adopted a same particle source profile for all discharges. The apparent fact that, in general, D_e is smaller for positive $\hat{s}$, is due to having such constant source profile while, in fact, the wall neutrals distribution should be changing with changing density gradients and puffing rates. In addition, discharges with negative induction ($\hat{s} < 0$) start generally with smaller densities precisely to avoid cut-off, but TJ-II ECRH plasmas are known to confine better the higher the density [**31**]. Examples of double ramps in the OH coils to prove that the confinement is indeed worse with positive plasma currents can be found on Ref. [**15**]. The ability to make these experiments with positive/negative I_p in one discharge makes evident that the density alone cannot explain the changes in confinement: as long as the effect on transport can be reversed by reversing the induction, the true knob for changing the transport cannot be the density but something related with the current. Three of such double ramp discharges are included in Figs. 15 and 16 with small crosses, open circles and open squares. In fact, the assumption of constant particle source can only be taken as a reasonable one for the highlighted discharges #7036 and #7046, where we can observe the trends in the whole range. Data from discharge #7046 are taken for $t > 1130$ to make it more comparable to discharge #7036 (see Fig. 3). The effect we want to focus in is that D_e decreases with the magnetic shear when $\hat{s} < 0$ but increases towards $\hat{s} = 0$. It is, however, difficult to conclude anything for $\hat{s} > 0$ because the achieved values of $\hat{s}$ are small due to starting from an already negative value in vacuum. The diffusivities in Fig. 15 seem to decrease again when $\hat{s} > 0$ and the trend afterwards seems to be towards larger diffusivity. Interestingly, the same plot using χ_e instead of D_e is qualitatively identical (Fig. 16).

6. *Discussion and conclusions*

Our experimental results can be briefly summarized: The parallel plasma conductivity in TJ-II ECRH plasmas is compatible with Spitzer's formula corrected by the fraction of passing particles. We have calculated the evolution of the rotational transform (and shear) provoked via induction of a plasma loop voltage. It is found that small changes in $\hat{s}$ alter the confinement. Negative shear in the density gradient region decreases particle and heat transport. Positive shear does not show a clear effect because the positive shear range explored is small, but at zero shear the transport appears to have a maximum. The location of low order

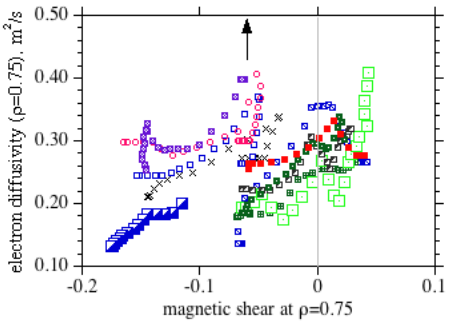

FIGURE 15. *Plot of the electron diffusivity at $\rho = 0.75$ versus the magnetic shear at the same position. Each symbol corresponds to an evolving discharge. Discharges #7036 and #7046 are highlighted with larger symbols. The vacuum value of $\hat{s}(0.75)$ is indicated with an arrow and all cases start from there.*

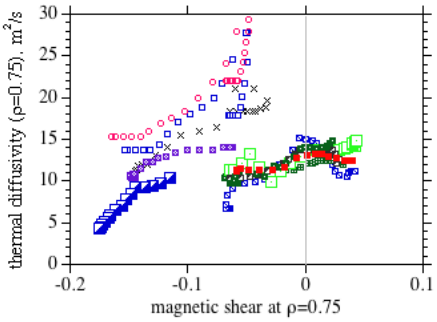

FIGURE 16. *Same as Fig. 15 for the electron thermal diffusivity.*

rationals is unimportant in these results, most likely due to having a finite, although small ($|\hat{s}| \gtrsim 0.1$), magnetic shear.

The heliac concept features large local shear while being almost shearless in the global sense [**13**]. In Ref. [**6**] it is argued that the radial extent of drift-wave modes are affected by local and global shear terms, the latter being comparably small especially when a stellarator with small $\hat{s}$ (like the TJ-II) is considered. The authors in Ref. [**6**] warn that, even being this the case, subdominant modes (e. g. related with toroidally trapped populations) may govern the nonlinear saturation of turbulence levels. Other authors have also been cautious to avow that the relative preponderance of local over global terms is proven when the latter are small, while the relative importance may be inverted for large $\hat{s}$ machines, like the heliotron [**41**, **7**, **8**]. The volume distribution of the local magnetic shear depends largely on the form of the nested magnetic flux surfaces. A moderate plasma current distribution that preserves the same nesting, as is our OH current, cannot change significantly the local shear distribution except for an *average* change of pitch of the magnetic field lines between neighboring flux surfaces, which amounts to the found variations in $\hat{s}$. We have checked that a flux surface dependent poloidal magnetic field consistent with a net plasma current of 20 kA does not modify the local shear map but negligibly. Even though global ($\hat{s}$) and local shear changes are linked, the key of these experiments is that the externally controllable average part of the shear can be correlated with particle and heat confinement.

Our results should encurage new calculations on microinstabilities with varying $\hat{s}$ around zero. Promising methods are available for this kind of numerical study [**42**]. However, and turning to our first comment on this paper, we are aware that the apparent link between $\hat{s}$ and confinement may be "contaminated" by other effects, like the modification of particle orbits, trapped particle fraction f_t and ECRH pump out [**43**] in the

presence of parallel electric fields, or the modification of radial electric fields depending on the radial position of low order ι rationals [**19**]. In [**16**] we argued that confinement changes respond to the plasma current but not to the induced electric field, which did not exclude contributions from the latter. Likewise, particle orbits can also be changed by modifying $\hat{s}$. We are performing calculations to investigate these aspects numerically. At the same time, new experiments are planned with a larger and upgraded set of diagnostics to seek for signals related to turbulence. This may help in discerning between the turbulence and the particle orbit pictures (if they can be separated!).

Acknowledgements

This work has been partly funded by the Spanish "Comisión Interministerial de Ciencia y Tecnología" under project FTN 2001-0688. We sincerely appreciate the help of Dr. G. V. Pereverzev in describing the geometry of TJ-II in the frame of ASTRA.

References

1. H. Maaßberg *et al.*, Phys. Fluids **B 5**, 3627 (1993).
2. J. Guasp, M. Liniers, Nuclear Fusion **40**, 397-411 (2000).
3. R. Brakel *et al.*, Plasma Phys. Control. Fusion **39**, B273-B286 (1997).
4. M. G. Shats *et al.*, Phys. Plasmas **2**, 398-413 (1995).
5. N. Dominguez, B. A. Carreras, V. E. Lynch, P. H. Diamond, Phys. Fluids **B4**, 2894 (1992).
6. R. E. Waltz, A. H. Boozer, Phys. Fluids B **5**, 2201 (1993).
7. N. Nadeem, T. Rafiq, M. Persson, Phys. Plasmas **8**, 4375 (2001).
8. A. Kendl, B. D. Scott, Phys. Rev. Lett. **90**, 035006 (2003).
9. T. Obiki *et al.*, in *Plasma Physics and Controlled Nuclear Fusion Research 1990* (Proc. 1th Int. Conf. Washington DC, 1990) Vol. II, p. 425, IAEA, Vienna (1991).
10. K. Nagasaki *et al.*, Phys. Plasmas **6**, 556-564 (1998).
11. S. Zoletnik *et al.*, Plasma Phys. Control. Fusion **44**, 1581-1607 (2002).
12. C. Alejaldre *et al.*, Fusion Technol. **17**, 131 (1990).
13. A. H. Boozer *et al.*, in *Plasma Physics and Controlled Nuclear Fusion Research 1982* (Proc. 9th Int. Conf. Baltimore, 1982), Vol. III, p. 129, IAEA, Vienna (1983).
14. E. Ascasíbar *et al.*, Plasma Phys. Control. Fusion **44**, B307 (2002).
15. J. A. Romero *et al.*, Nucl. Fusion **43**, 387 (2003).
16. D. López-Bruna *et al.*, Nucl. Fusion **44**, 645 (2004).
17. T. Estrada *et al.*, Plasma Phys. Control. Fusion **44**, 1615 (2002).
18. T. Estrada *et al.*, Plasma Phys. Control. Fusion **46**, 277 (2004).
19. F. Castejón *et al.*, Nucl. Fusion **44**, 593 (2004).
20. A. Fujisawa, Plasma Phys. Control. Fusion **45**, R1-R88 (2003).
21. I. García-Cortés *et al.*, Nucl. Fusion **40**, 1867 (2000).
22. D. W. Atkinson *et al.*, in *Plasma Physics and Controlled Nuclear Fusion Research 1980* (IAEA, Vienna 1981) Vol. I, p. 161.
23. H. Ringler *et al.*, Plasma Phys. Controll. Fusion **32**(11), 913 (1990).
24. F. Castejón *et al.*, Bull. Am. Phys. Soc. **36** 3S 27, 2343 (1991).
25. A. Baciero *et al.*, Plasma Phys. Control. Fusion **43**, 1039 (2001).
26. V. Tribaldos, Phys. Plasmas **8** (4), 1229-1239 (2001).
27. A. Rodríguez-Yunta, *Neoclassical studies in Heliac TJ-II*, Proc. 8th Int. Workshop on Stellarators, IAEA Technical Committee Meeting (Kharkov USSR) 1991, p. 69.
28. J. A. Jimenez, *Bootstrap Current Studies in the TJ-II Heliac*, Proc. 27th EPS Conference on Controlled Fusion and Plasma Physics, Budapest, 12-16 June 2000, ECA Vol. 24B, 197-200 (2000).
29. V. Tribaldos, H. Maaßberg, J. A. Jiménez, A. Varias, *Bootstrap Current Simulations for the TJ-II Stellarator*, Proc. 30th EPS Conference on Contr. Fusion and Plasma Phys., St. Petersburg, 7-11 July 2003, ECA Vol. 27A, P-1.28 (2003).
30. D. T. Anderson *et al.*, in *Plasma Physics and Controlled Nuclear Fusion Research 1982* (IAEA, Vienna 1983) Vol. III, p. 105.
31. E. Ascasíbar *et al.*, Nucl. Fusion **45**, 276-284 (2005).
32. G. V. Pereverzev *et al.*, *ASTRA: an Automatic System for Transport Analysis*, Max-Planck-Institut für Plasmaphysik, Rep. IPP 5142, Garching (1991).
33. A. López-Fraguas, D. López-Bruna, J. A. Romero, *Cálculo del potencial magnético vector en el TJ-II*, Informes Técnicos CIEMAT n° 1055 (2005) (in Spanish).
34. D. K. Akulina *et al.*, in *Plasma Physics and Controlled Nuclear Fusion Research 1978* (Proc. 7th. Int. Conf. Innsbruck, 1978), Vol. II, p. 287, IAEA, Vienna (1978).

35. J. M. Fontdecaba *et al.*, Fusion Sci. Tech. **46**, 271 (2004).
36. E. de la Luna *et al.*, Rev. Sci. Intrum. **72**, 379 (2001).
37. J. Herranz, F. Castejón, I. Pastor, K. McCarthy, Fusion Eng. Des. **65** (4) 525-536, (2003).
38. K. C. Shaing, J. D. Callen, Phys. Fluids **26**, 3315 (1983).
39. A. Varias, J. A. Jiménez, A. López-Fraguas, F. Castejón, *Stability properties of stellarators with a net toroidal current*, Proc. 15th Int. School of Plasma Physics, Varenna 1994, Theory of Fusion Plasmas (1994), 379.
40. F. L. Tabarés *et al.*, Plasma Phys. Control. Fusion **43**, 1023-1037 (2001).
41. A. Kendl, H. Wobig, Phys. Plasmas **6**, 12, 4714 (1999).
42. L. Villard *et al*, Nucl. Fusion **44**, 172-180 (2004).
43. M. A. Ochando, F. Medina, Plasma Phys. Control. Fusion **45** 221 (2003).

Informes Técnicos Ciemat **1089**
Septiembre, 2006

Magnetic Shear and Transport in ECRH Discharges of the TJ-II under Ohmic Induction

D. López-Bruna
F. Castejón
J. A. Romero
T. Estrada
F. Medina
M. Ochando
A. López-Fraguas
E. Ascasíbar
J. Herranz
E. Sánchez
E. de la Luna
I. Pastor

Laboratorio Nacional de Fusión por Confinamiento Magnético

Magnetic Shear and Transport in ECRH Discharges of the TJ-II under Ohmic Induction.

López-Bruna, D.; Castejón, F.; Romero, J.A.; Estrada, T.; Medina, F.; Ochando, M.;
López-Fraguas, A.; Ascasíbar, E.; Herranz, J.; Sánchez, E.; de la Luna, E.; Pastor, I.

17 pp. 16 figs. 43 refs.

Abstract:
TJ-II is a heliac type stellarator characterised by high, but almost constant, vacuum rotational transform throughout the confining volume. In ECRH plasmas, moderate induced ohmic currents (negligible heating and modification of the magnetic field rnodulus) are enough to disregard the bootstrap contribution, which allows us performing a fair calculation of the evolution of the rotational transform. We use the loop voltage diagnostic to estimate the plasma electrical conductivity. Then the evolution of the rotational transform and shear is related to changes in the profiles of electron and thermal diffusivities: negativo shear correlates with decreasing diffusivities in the region of steepest density gradient; transport increases toward zero shear but the achieved positive values are too small to draw conclusions. The radial sweeping of lowest order rational magnetic surfaces does not determine the observed trends in transport.

Cizalla Magnética y Transporte en Descargas ECRH del TJ-II con Inducción Óhmica.

López-Bruna, D.; Castejón, F.; Romero, J.A.; Estrada, T.; Medina, F.; Ochando, M.;
López-Fraguas, A.; Ascasíbar, E.; Herranz, J.; Sánchez, E.; de la Luna, E.; Pastor, I.

17 pp. 16 figs. 43 refs.

Resumen:
Una característica del TJ-II, un estelarador tipo *heliac,* es su alta y cuasiconstante transformada rotacional de vacío. Puesto que, en los plasmas ECRH, pequeñas corrientes inducidas (que apenas alteran la inducción magnética o el calentamiento) bastan para despreciar la corriente de *bootstrap,* la evolución de la transformada rotacional puede calcularse bien. Tras estimar la conductividad eléctrica del plasma mediante el diagnóstico de voltaje inducido, relacionamos la evolución de la transformada rotacional y de su cizalla con cambios en los perfiles de las diíusividades electrónica y térmica electrónica: en la zona de gradiente de la densidad se tiene menor difusividad a mayor cizalla negativa; cerca de la cizalla nula el transporte aumenta, pero luego los valores positivos alcanzados no permiten sacar conclusiones. Estas tendencias no surgen del movimiento de superficies magnéticas singulares a través del plasma.

CLASIFICACIÓN DOE Y DESCRIPTORES

S70
SHEAR; ELECTRON CYCLOTRON-RESONANCE; PLASMA HEATING; TOKAMAK DEVICES; ROTATIONAL TRANSFORM; DENSITY; HELIAC STELLARATORS

Magnetic Shear and Transport in ECRH Discharges of the TJ-II under Ohmic Induction.

López-Bruna, D.; Castejón, F.; Romero, J.A.; Estrada, T.; Medina, F.; Ochando, M.;
López-Fraguas, A.; Ascasíbar, E.; Herranz, J.; Sánchez, E.; de la Luna, E.; Pastor, I.

17 pp. 16 figs. 43 refs.

Abstract:
TJ-II is a heliac type stellarator characterised by high, but almost constant, vacuum rotational transform throughout the confining volume. In ECRH plasmas, moderate induced ohmic currents (negligible heating and modification of the magnetic field rnodulus) are enough to disregard the bootstrap contribution, which allows us performing a fair calculation of the evolution of the rotational transform. We use the loop voltage diagnostic to estimate the plasma electrical conductivity. Then the evolution of the rotational transform and shear is related to changes in the profiles of electron and thermal diffusivities: negativo shear correlates with decreasing diffusivities in the region of steepest density gradient; transport increases toward zero shear but the achieved positive values are too small to draw conclusions. The radial sweeping of lowest order rational magnetic surfaces does not determine the observed trends in transport.

Cizalla Magnética y Transporte en Descargas ECRH del TJ-II con Inducción Óhmica.

López-Bruna, D.; Castejón, F.; Romero, J.A.; Estrada, T.; Medina, F.; Ochando, M.;
López-Fraguas, A.; Ascasíbar, E.; Herranz, J.; Sánchez, E.; de la Luna, E.; Pastor, I.

17 pp. 16 figs. 43 refs.

Resumen:
Una característica del TJ-II, un estelarador tipo *heliac,* es su alta y cuasiconstante transformada rotacional de vacío. Puesto que, en los plasmas ECRH, pequeñas corrientes inducidas (que apenas alteran la inducción magnética o el calentamiento) bastan para despreciar la corriente de *bootstrap,* la evolución de la transformada rotacional puede calcularse bien. Tras estimar la conductividad eléctrica del plasma mediante el diagnóstico de voltaje inducido, relacionamos la evolución de la transformada rotacional y de su cizalla con cambios en los perfiles de las diíusividades electrónica y térmica electrónica: en la zona de gradiente de la densidad se tiene menor difusividad a mayor cizalla negativa; cerca de la cizalla nula el transporte aumenta, pero luego los valores positivos alcanzados no permiten sacar conclusiones. Estas tendencias no surgen del movimiento de superficies magnéticas singulares a través del plasma.

CLASIFICACIÓN DOE Y DESCRIPTORES

S70
SHEAR; ELECTRON CYCLOTRON-RESONANCE; PLASMA HEATING; TOKAMAK DEVICES; ROTATIONAL TRANSFORM; DENSITY; HELIAC STELLARATORS